

Article

Not peer-reviewed version

A Dynamic Inverse Decoupling Control Method for Reducing Energy Consumption in Quadcopter UAV

[Guoxin Ma](#)*, [Kang Tian](#), [Hongbo Sun](#), Yongyan Wang, [Haitao Li](#)

Posted Date: 24 March 2025

doi: 10.20944/preprints202503.1607.v1

Keywords: quadrotor UAV; low-energy consumption; dynamics; decoupling control



Preprints.org is a free multidisciplinary platform providing preprint service that is dedicated to making early versions of research outputs permanently available and citable. Preprints posted at Preprints.org appear in Web of Science, Crossref, Google Scholar, Scilit, Europe PMC.

Copyright: This open access article is published under a Creative Commons CC BY 4.0 license, which permit the free download, distribution, and reuse, provided that the author and preprint are cited in any reuse.

Article

A Dynamic Inverse Decoupling Control Method for Reducing Energy Consumption in Quadcopter UAV

Guoxin Ma ^{1,*}, Kang Tian ¹, Hongbo Sun ¹, Yongyan Wang ² and Haitao Li ²

¹ School of Computer and Control Engineering, Yantai University, Yantai, 264005, China; 2681907457@qq.com (K.T.); sunhongbo02@tsinghua.org.cn (H.B.S.)

² Beijing Institute of Environmental Features, China Aerospace Science and Industry Corporation, Beijing 100161, China; sunday10200725@163.com (Y.Y.W.); li_ht207@126.com (H.T.L.)

* Correspondence: ma_guoxin@163.com

Abstract: The energy consumption of rotary wing unmanned aerial vehicles has become an important factor restricting their long-term application. This article focuses on decoupling the motion channel and reducing control energy consumption, and proposes a decoupling controller based on dynamic inversion for the complete dynamics of quadcopter unmanned aerial vehicles. Firstly, design a direct closed-loop feedback control for the z-channel to exhibit second-order linear dynamic characteristics with adjustable parameters. Then, the specific functions of pitch angle and yaw angle are combined as virtual control variables for the comprehensive decoupling design of x-direction and y-direction, so that the x-channel and y-channel also exhibit independent parameter adjustable second-order linear dynamic characteristics. Next, by solving the actual control variables, a fast convergence system is dynamically formed by the deviation between the virtual control variables and their actual values, ensuring that the specific function combination of pitch angle and yaw angle quickly converges to the expected value. Finally, the effectiveness and low energy consumption control characteristics of the decoupling control scheme were demonstrated through simulation comparison with other control methods (such as classical PID) in terms of energy consumption.

Keywords: Quadrotor UAV; Low-energy consumption; Dynamics; Decoupling Control

1. Introduction

The quadrotor UAV has been widely applied in both military and civil fields. Its advantages, such as good stability, flexible takeoff and landing, and simple control, make it frequently used in tasks such as search and rescue [1–3], inspection [4,5], surveying [6–8], and aerial photography [9–11]. However, compared to fixed-wing UAVs, rotorcraft UAVs have relatively limited endurance due to their propulsion characteristics and onboard energy constraints—its energy is extremely limited and consumed quickly [12–14]. This challenge has become an important issue that current and future researchers need to address.

To improve the endurance of rotorcraft UAVs, researchers not only need to focus on developing more efficient energy storage devices but also need to optimize flight control strategies to avoid unnecessary energy waste. Recent studies have started exploring ways to enhance the flight efficiency of quadrotor UAVs through advanced control algorithms and path planning techniques [15–19].

Due to the strong nonlinearity, underactuation, and coupling characteristics exhibited by the dynamic model of quadrotor UAVs, researchers in recent years have proposed various control strategies based on nonlinear design methods. These strategies include backstepping design [20,21], sliding mode control [22–24], H- ∞ control [25,26], adaptive control [27–29], fuzzy control [30,31], as well as combinations of multiple control methods. However, while these studies focus on achieving optimal control performance, they often overlook the issue of energy consumption during the actual

control process of the rotorcraft UAV. This oversight leads to excessive energy consumption, which limits the UAV's endurance and scope of application.

In current implementations of quadrotor UAV control, some recent studies have started to focus on reducing energy consumption right from the beginning of the control strategy design, aiming to extend the UAV's endurance and expand its range of applications [32].

The above methods focus on their respective research themes, either targeting control performance or optimizing specific issues (such as local path optimization or attitude control optimization), without making the reduction of control energy consumption the central goal. These methods do not directly address the full dynamics of the quadrotor UAV, nor do they perform integrated position and attitude control from the initial point to the target point. Furthermore, energy optimization for the quadrotor UAV, from the initial position to the target position, is mathematically equivalent to the minimum fuel control problem of a double integrator model, and optimal control design based on the HJB (Hamilton-Jacobi-Bellman) equation [33] inevitably leads to control strategies resembling Bang-Bang control or its variants. However, unlike ground vehicles, UAVs in the air cannot adopt the "acceleration-glide-deceleration" technique for energy saving. Specifically, inertial movement with zero control input in the middle of the flight from the initial to the target position is highly unsafe for flight control. To address this issue, this paper avoids the traditional optimal control design approach based on the HJB equation and instead transforms the reduction of energy consumption into the design and realization of desired dynamics. The main contributions are as follows:

1. **Dynamic Inverse Feedback Controller Design:** We designed a novel dynamic inverse feedback controller for the full dynamics of the quadrotor UAV, which can achieve dynamic decoupling of the UAV's x/y/z channels.

2. **Integration of Initial and Terminal Conditions:** During continuous and safe flight control, we incorporate initial and terminal conditions that affect optimality into the desired dynamic design of the x/y/z channels, transforming the energy consumption reduction problem into a discussion of the dynamic synchronization and damping characteristics of the x/y/z channels.

3. **Significant Reduction in Energy Consumption:** Compared to typical control methods, the designed dynamic inverse decoupling controller greatly reduces control energy consumption and offers convenient editability of the desired dynamics for each channel.

2. Methodology

This section first establishes the dynamic model of the quadrotor UAV, then presents the UAV energy consumption model, and finally derives the dynamic inverse decoupling control method proposed in this paper.

2.1. Quadrotor UAV Dynamic Modeling

To clearly describe the control design method of this article, we use a cross shaped coaxial quadcopter unmanned aerial vehicle as the research object. It should be noted that the design idea of this article is not limited to this, and can also be applied to other configurations of multi rotor unmanned aerial vehicles.

According to the layout, quadcopter drones can be divided into two architectures: a "cross" shaped and an "X" shaped. The direction of the cross shaped drone nose is consistent with the direction of one of the rotors; The "X" shaped drone nose points towards the middle of two adjacent rotors. The research object of this article is a "cross" shaped quadcopter unmanned aerial vehicle, and its fuselage structure is shown in Figure 1.

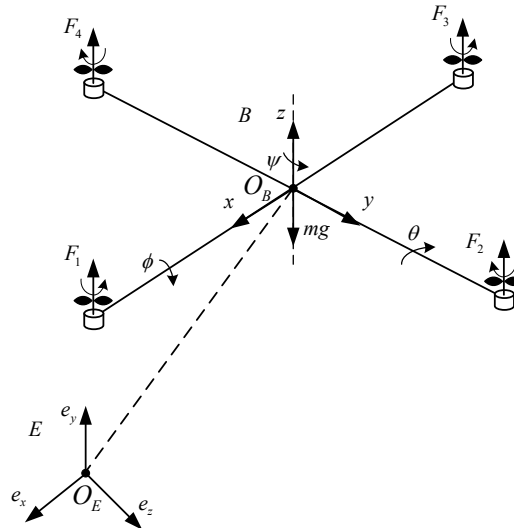


Figure 1. Quadcopter drone fuselage structure.

where $E(e_x, e_y, e_z)$ represents the ground coordinate system, $B(x, y, z)$ represents the body coordinate system. The lift generated by motors 1 to 4 is F_1 to F_4 , respectively. ϕ represents the roll angle of the drone around the x -axis, θ represents the pitch angle of the drone around the y -axis, ψ represents the yaw angle of the drone around the z -axis, that is, the Euler angle of the quadcopter drone in the Z - Y - X rotation sequence is $[\phi, \theta, \psi]$.

Using a ground coordinate system, the dynamic model of a quadcopter drone can be represented as Equation (1)[34]:

$$\begin{cases} \ddot{x} = \frac{u_1}{m} [\cos \phi \sin \theta \cos \psi + \sin \phi \sin \psi] - \frac{K_x \dot{x}}{m} \\ \ddot{y} = \frac{u_1}{m} [\cos \phi \sin \theta \sin \psi - \sin \phi \cos \psi] - \frac{K_y \dot{y}}{m} \\ \ddot{z} = \frac{u_1}{m} \cos \phi \cos \theta - g - \frac{K_z \dot{z}}{m} \\ \ddot{\phi} = \frac{(I_y - I_z)}{I_x} \dot{\theta} \dot{\psi} + \frac{J_r}{I_x} \dot{\theta} \dot{\Omega}_r + \frac{u_2 l}{I_x} - \frac{K_\phi l}{I_x} \dot{\phi} \\ \ddot{\theta} = \frac{(I_z - I_x)}{I_y} \dot{\phi} \dot{\psi} - \frac{J_r}{I_y} \dot{\phi} \dot{\Omega}_r + \frac{u_3 l}{I_y} - \frac{K_\theta l}{I_y} \dot{\theta} \\ \ddot{\psi} = \frac{(I_x - I_y)}{I_z} \dot{\phi} \dot{\theta} + \frac{u_4}{I_z} - \frac{K_\psi}{I_z} \dot{\psi} \end{cases} \quad (1)$$

where x, y, z indicate the center of gravity position of the quadcopter drone, ϕ, θ, ψ representing the roll, pitch, and yaw angles of the drone, respectively, and $\phi \in (-\pi/2, \pi/2)$, $\theta \in (-\pi/2, \pi/2)$, $\psi \in (-\pi, \pi)$. m indicate the quality of the drone, g representing gravitational acceleration, l indicate the distance from the center of each rotor to the center of gravity. u_1, u_2, u_3, u_4 indicate the control input quantity of the drone, J_r indicating the rotational inertia of the propeller, I_x, I_y, I_z indicate the moment of inertia of the drone in the x, y and z axes, $K_x, K_y, K_z, K_\phi, K_\theta, K_\psi$ representing drag coefficient, Ω_r indicate the linear combination of motor speed.

where $u_1 = F_1 + F_2 + F_3 + F_4$, $u_2 = -F_2 + F_4$, $u_3 = -F_1 + F_3$, $u_4 = d(-F_1 + F_2 - F_3 + F_4)/b$, $F_i = b\Omega_i^2$ indicate the lift of each rotor of the drone, Ω_i indicate the speed of each motor, b indicate the lift coefficient, d indicate the proportional coefficient of torque, $\Omega_r = -\Omega_1 + \Omega_2 - \Omega_3 + \Omega_4$.

From this, it can be inferred that the relationship between rotational speed and control quantity is:

$$\begin{aligned}
 \Omega_1 &= \sqrt{\Omega_3^2 - \frac{u_3}{b}} \\
 \Omega_2 &= \sqrt{\Omega_4^2 - \frac{u_2}{b}} \\
 \Omega_3 &= \sqrt{\frac{u_1 + u_2 + u_3}{2b} - \Omega_4^2} \\
 \Omega_4 &= \sqrt{\frac{u_1}{2b} + \frac{u_2}{b} + \frac{u_4}{2d}}
 \end{aligned} \quad (2)$$

2.2. UAV Energy Consumption Model

2.2.1. Analysis of UAV Energy Consumption Model

The energy consumption model of unmanned aerial vehicles is a mathematical description that quantifies the energy consumption of unmanned aerial vehicles during flight. This section presents experimental data in the form of charts based on measured data of unmanned aerial vehicles, in order to establish a more accurate and realistic energy consumption model for unmanned aerial vehicles. The actual test scenario is shown in Figure 2.

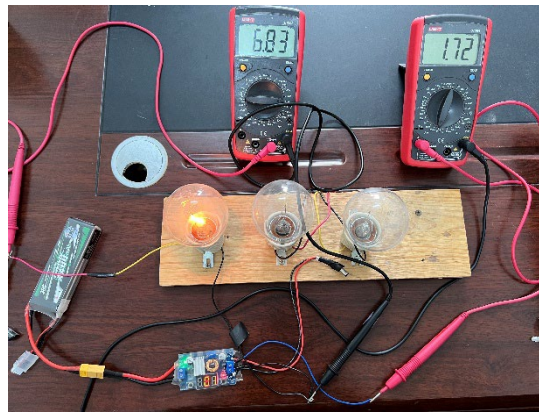


Figure 2. UAV energy consumption measurement scenario.

The parameters of the quadcopter unmanned aerial vehicle used in this article are shown in Table 1. In actual testing, after measuring voltage and current, the power is obtained according to the formula, and the variation law of power with time can be obtained from the curve graph of power and time. There are a total of 5 sets of data in this test, and the final set of test data obtained through integration is shown in Figure 3.

Table 1. Drone energy consumption testing parameters.

Name	Specific parameters
battery	12V (4V * 3 sections)
bare weight	1.8kg
fixed load power	100w

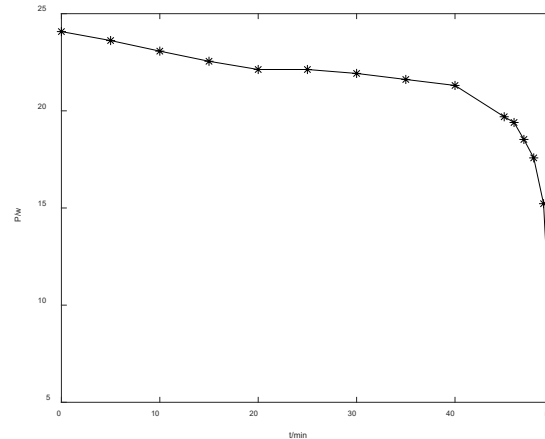


Figure 3. Changes in drone power and time.

2.2.2. Establishment of drone energy consumption model

The drone energy consumption model is a mathematical description that quantifies the energy consumption of drones during flight, used to analyze the energy consumption characteristics under different flight conditions and mission scenarios. The energy consumption model is an important foundation for optimizing drone mission planning, flight control, and energy management. Its construction requires comprehensive consideration of various factors such as flight dynamics, mission load, and environmental conditions. This section is based on the results of Figure 3 to model the energy consumption of unmanned aerial vehicles [35].

The force generated by the rotation of rotor i at time t can be expressed as:

$$F_i(t) = b\Omega_i^2(t) \quad (3)$$

Define $U_i(t)$ as the voltage of the motor corresponding to rotor i at time t , and $I_i(t)$ as the current of the motor corresponding to rotor i at time t . The expansion equations are:

$$U_i(t) = \frac{30K_E\Omega_i(t)}{\pi} + I_i(t)R_0 \quad (4)$$

$$I_i(t) = \frac{\Omega_i^2(t)}{K_M} + I_0 \quad (5)$$

where K_E represents the back electromotive force constant of the motor, $K_E \triangleq \frac{U_0 - I_0 R_0}{380U_0}$, K_M represents the torque constant, $K_M \triangleq 9.55K_E$, U_0 , I_0 , R_0 respectively represent the no-load voltage, current, and resistance of the motor.

For the motor loaded on rotor i , the power at time t can be expressed as:

$$P_i(t) = U_i(t)I_i(t) \quad (6)$$

The power expression can be further expanded as:

$$P_i(t) = r_1\Omega_i^4(t) + r_2\Omega_i^3(t) + r_3\Omega_i^2(t) + r_4\Omega_i(t) + I_0^2 R_0 \quad (7)$$

where:

$$r_1 = \frac{R_0}{b^2}, r_2 = \frac{30K_E}{\pi b}, r_3 = \frac{2I_0 R_0}{b}, r_4 = \frac{30K_E I_0}{\pi} \quad (8)$$

Assuming that the rotor angular velocity of the drone at time t is $\Omega_c = \Omega_v(t)$ at speed v_c , the total flight power $p_v(t)$ of the drone at speed v_c can be obtained as:

$$P_v(t) = 4U_v(t)I_v(t) = 4(r_1\Omega_c^4 + r_2\Omega_c^3 + r_3\Omega_c^2 + r_4\Omega_c + I_0^2 R_0) \quad (9)$$

The flight energy consumption $E_v(t)$ of the drone at time t can be expressed as:

$$E_v(t) = \int_0^t P_v(t) dt \quad (10)$$

2.3. Dynamic Inverse Decoupling Control Method

Firstly, design a direct closed-loop feedback control for the z -channel to exhibit second-order linear dynamic characteristics with adjustable parameters. Then, the specific functions of pitch angle and yaw angle are combined as virtual control variables for the comprehensive decoupling design of x -direction and y -direction, so that the x -channel and y -channel also exhibit independent parameter adjustable second-order linear dynamic characteristics. Next, by solving the actual control variables, a fast convergence system is dynamically formed by the deviation between the virtual control variables and their actual values, ensuring that the specific function combination of pitch angle and yaw angle quickly converges to the expected value.

The specific process of designing a dynamic inverse decoupling control strategy for a quadcopter unmanned aerial vehicle based on Equation (1) is as follows:

The control input u_1 is set to:

$$u_1 = \frac{m}{\cos \phi \cos \theta} \left[\ddot{z}^d + \frac{K_z}{m} \dot{z}^d + a_3 \dot{e}_z + b_3 e_z + g \right] \quad (11)$$

where z^d indicate the expected target point of z , $e_z = z^d - z$, $\dot{e}_z = \dot{z}^d - \dot{z}$.

By taking the derivative of u_1 , we can obtain:

$$\begin{aligned} \dot{u}_1 = & \frac{m \left[\dot{\phi} \sin \phi \cos \theta + \dot{\theta} \cos \phi \sin \theta \right]}{[\cos \phi \cos \theta]^2} \left[\ddot{z}^d + \frac{K_z}{m} \dot{z}^d + a_3 \dot{e}_z + b_3 e_z + g \right] \\ & + \frac{m}{\cos \phi \cos \theta} \left[\ddot{z}^d + \frac{K_z}{m} \dot{z}^d + a_3 \dot{e}_z + b_3 e_z \right] \end{aligned} \quad (12)$$

where $\ddot{e}_z = \ddot{z}^d - \ddot{z}$, $\dot{z} = \frac{1}{m} (\cos \phi \cos \theta) u_1 - g - \frac{K_z \dot{z}}{m}$.

Equation (11) can make z dynamic as:

$$\ddot{e}_z + \left(a_3 + \frac{K_z}{m} \right) \dot{e}_z + b_3 e_z = 0 \quad (13)$$

If x and y generate synchronous dynamics, it is possible to achieve straight-line flight from the initial point to the target point. According to the dynamic model, it can be inferred that:

$$\begin{bmatrix} \ddot{x} \\ \ddot{y} \end{bmatrix} = \frac{u_1}{m} \begin{bmatrix} \cos \psi & \sin \psi \\ \sin \psi & -\cos \psi \end{bmatrix} \begin{bmatrix} \cos \phi \sin \theta \\ \sin \phi \end{bmatrix} - \begin{bmatrix} \frac{K_x \dot{x}}{m} \\ \frac{K_y \dot{y}}{m} \end{bmatrix} \quad (14)$$

Define x^d, y^d as the expected target point for x and y , $e_x = x^d - x$, $e_y = y^d - y$, $\dot{e}_x = \dot{x}^d - \dot{x}$, $\dot{e}_y = \dot{y}^d - \dot{y}$, $\ddot{e}_x = \ddot{x}^d - \ddot{x}$, $\ddot{e}_y = \ddot{y}^d - \ddot{y}$. Set expectations:

$$\begin{cases} \ddot{e}_{xdesired} = -\left(a_1 + \frac{K_x}{m} \right) \dot{e}_x - b_1 e_x \\ \ddot{e}_{ydesired} = -\left(a_2 + \frac{K_y}{m} \right) \dot{e}_y - b_2 e_y \end{cases} \quad (15)$$

If the function $[\cos \phi \sin \theta \sin \phi]^T$ of ϕ, θ is treated as a virtual control variable and Equation (15) holds, then:

$$\frac{u_1}{m} \begin{bmatrix} \cos \psi & \sin \psi \\ \sin \psi & -\cos \psi \end{bmatrix} \left\{ \begin{bmatrix} \cos \phi \sin \theta \\ \sin \phi \end{bmatrix} \right\}_{desired} - \begin{bmatrix} \frac{K_x \dot{x}}{m} \\ \frac{K_y \dot{y}}{m} \end{bmatrix} = \begin{bmatrix} \ddot{x}^d + \left(a_1 + \frac{K_x}{m} \right) \dot{e}_x + b_1 e_x \\ \ddot{y}^d + \left(a_2 + \frac{K_y}{m} \right) \dot{e}_y + b_2 e_y \end{bmatrix} \quad (16)$$

Setting $f_1 = \cos \phi \sin \theta$, $f_2 = \sin \phi$, their expected values are denoted as \bar{f}_1, \bar{f}_2 , then rewrite Equation (16) as:

$$\begin{bmatrix} \bar{f}_1 \\ \bar{f}_2 \end{bmatrix} = \frac{m}{u_1} \begin{bmatrix} \cos \psi & \sin \psi \\ \sin \psi & -\cos \psi \end{bmatrix}^{-1} \begin{bmatrix} \ddot{x}^d + \frac{K_x}{m} \dot{x}^d + a_1 \dot{e}_x + b_1 e_x \\ \ddot{y}^d + \frac{K_y}{m} \dot{y}^d + a_2 \dot{e}_y + b_2 e_y \end{bmatrix} \quad (17)$$

Definition $E_{\phi, \theta} = [\bar{f}_1 \bar{f}_2]^T - [f_1 f_2]^T$, by exerting control $E_{\phi, \theta} \rightarrow 0$, order $\ddot{E}_{\phi, \theta} + A \dot{E}_{\phi, \theta} + B E_{\phi, \theta} = 0$. And:

$$A = \begin{bmatrix} a_{11} & 0 \\ 0 & a_{22} \end{bmatrix}, B = \begin{bmatrix} b_{11} & 0 \\ 0 & b_{22} \end{bmatrix} \quad (18)$$

Substituting can rewrite $\ddot{E}_{\phi,\theta} + A\dot{E}_{\phi,\theta} + BE_{\phi,\theta} = 0$ as:

$$\begin{aligned} (\ddot{f}_1 - \ddot{f}_1) + a_{11}(\dot{f}_1 - \dot{f}_1) + b_{11}(\bar{f}_1 - f_1) &= 0 \\ (\ddot{f}_2 - \ddot{f}_2) + a_{22}(\dot{f}_2 - \dot{f}_2) + b_{22}(\bar{f}_2 - f_2) &= 0 \end{aligned} \quad (19)$$

Equation (19) can be further divided and organized into:

$$\ddot{f}_1 - \ddot{f}_1 = a_{11}(\dot{f}_1 - \dot{f}_1) + b_{11}(\bar{f}_1 - f_1) \quad (20)$$

$$\ddot{f}_2 - \ddot{f}_2 = a_{22}(\dot{f}_2 - \dot{f}_2) + b_{22}(\bar{f}_2 - f_2) \quad (21)$$

Equation (17) can be organized as:

$$\bar{f}_1 = \frac{m}{u_1} \left[\cos\psi \left(\ddot{x}^d + \frac{K_x}{m} \dot{x}^d + a_1 \dot{e}_x + b_1 e_x \right) + \sin\psi \left(\ddot{y}^d + \frac{K_y}{m} \dot{y}^d + a_2 \dot{e}_y + b_2 e_y \right) \right] \quad (22)$$

$$\bar{f}_2 = \frac{m}{u_1} \left[\sin\psi \left(\ddot{x}^d + \frac{K_x}{m} \dot{x}^d + a_1 \dot{e}_x + b_1 e_x \right) - \cos\psi \left(\ddot{y}^d + \frac{K_y}{m} \dot{y}^d + a_2 \dot{e}_y + b_2 e_y \right) \right] \quad (23)$$

Setting $f_x = \ddot{x}^d + \frac{K_x}{m} \dot{x}^d + a_1 \dot{e}_x + b_1 e_x$, $f_y = \ddot{y}^d + \frac{K_y}{m} \dot{y}^d + a_2 \dot{e}_y + b_2 e_y$, $g_{\psi,x,y} = \cos\psi f_x + \sin\psi f_y$, $h_{\psi,x,y} = \sin\psi f_x - \cos\psi f_y$,

Equations (22) and (23) can be rewritten as:

$$\bar{f}_1 = u_1^{-1} m g_{\psi,x,y} \quad (24)$$

$$\bar{f}_2 = u_1^{-1} m h_{\psi,x,y}$$

Derive f_2 and \bar{f}_2 , substitute \ddot{f}_2 and \dot{f}_2 into Equation (21), and organize them to obtain:

$$\ddot{\phi} T_{1a} + \dot{\theta} T_{1b} = T_{1c} \quad (25)$$

where T_{1a} , T_{1b} , T_{1c} is:

$$\begin{aligned} T_{1a} &= \cos\phi + m^2 h_{\psi,x,y} u_1^{-2} u_1^B \sin\phi \cos\theta / (\cos\phi \cos\theta)^2 \\ T_{1b} &= m^2 h_{\psi,x,y} u_1^{-2} u_1^B \cos\phi \sin\theta / (\cos\phi \cos\theta)^2 \\ T_{1c} &= a_{22}(\ddot{f}_2 - \dot{f}_2) + b_{22}(\bar{f}_2 - f_2) - 2u_1^{-2} \dot{u}_1 m \dot{h}_{\psi,x,y} \\ &\quad + u_1^{-1} m \ddot{h}_{\psi,x,y} + \dot{\phi}^2 \sin\phi + 2u_1^{-3} \dot{u}_1^2 m h_{\psi,x,y} \\ &\quad - m^2 h_{\psi,x,y} u_1^{-2} u_1^B (\dot{\phi}^2 \cos\phi \cos\theta - 2\dot{\phi}\dot{\theta} \sin\phi \sin\theta \\ &\quad + \dot{\theta}^2 \cos\phi \cos\theta) / (\cos\phi \cos\theta)^2 \\ &\quad - 2m^2 h_{\psi,x,y} u_1^{-2} u_1^B (\dot{\phi} \sin\phi \cos\theta + \dot{\theta} \cos\phi \sin\theta)^2 / (\cos\phi \cos\theta)^3 \\ &\quad - m h_{\psi,x,y} u_1^{-2} (u_1^A \dot{u}_1^B + \dot{u}_1^C u_1^D + u_1^C \dot{u}_1^D) \end{aligned} \quad (26)$$

Derive f_1 and \bar{f}_1 , substitute \ddot{f}_1 and \dot{f}_1 into Equation (20), and organize them to obtain:

$$\ddot{\phi} T_{2a} + \dot{\theta} T_{2b} = T_{2c} \quad (27)$$

where T_{2a} , T_{2b} , T_{2c} is:

$$\begin{aligned} T_{2a} &= m^2 g_{\psi,x,y} u_1^{-2} u_1^B \sin\phi \cos\theta / (\cos\phi \cos\theta)^2 - \sin\phi \sin\theta \\ T_{2b} &= \cos\phi \cos\theta + m^2 g_{\psi,x,y} u_1^{-2} u_1^B \cos\phi \sin\theta / (\cos\phi \cos\theta)^2 \\ T_{2c} &= a_{11}(\ddot{f}_1 - \dot{f}_1) + b_{11}(\bar{f}_1 - f_1) + 2m g_{\psi,x,y} u_1^{-3} \dot{u}_1^2 - u_1^{-2} \dot{u}_1 m \dot{g}_{\psi,x,y} \\ &\quad - u_1^{-2} \dot{u}_1 m \dot{g}_{\psi,x,y} + u_1^{-1} m \ddot{g}_{\psi,x,y} + \dot{\phi}^2 \cos\phi \sin\theta + 2\dot{\phi}\dot{\theta} \sin\phi \cos\theta \\ &\quad + \dot{\theta}^2 \cos\phi \sin\theta - m^2 g_{\psi,x,y} u_1^{-2} u_1^B (\dot{\phi}^2 \cos\phi \cos\theta - 2\dot{\phi}\dot{\theta} \sin\phi \sin\theta \\ &\quad + \dot{\theta}^2 \cos\phi \cos\theta) / (\cos\phi \cos\theta)^2 \\ &\quad - 2m^2 g_{\psi,x,y} u_1^{-2} u_1^B (\dot{\phi} \sin\phi \cos\theta + \dot{\theta} \cos\phi \sin\theta)^2 / (\cos\phi \cos\theta)^3 \\ &\quad - m g_{\psi,x,y} u_1^{-2} (u_1^A \dot{u}_1^B + \dot{u}_1^C u_1^D + u_1^C \dot{u}_1^D) \end{aligned} \quad (28)$$

where u_1^A , u_1^B , u_1^C , u_1^D is:

$$u_1^A = \frac{m \left[\dot{\phi} \sin \phi \cos \theta + \dot{\theta} \cos \phi \sin \theta \right]}{[\cos \phi \cos \theta]^2}$$

$$u_1^B = \ddot{z}^d + \frac{K_z}{m} \dot{z}^d + a_3 \dot{e}_z + b_3 e_z + g \quad (29)$$

$$u_1^C = \frac{m}{\cos \phi \cos \theta}$$

$$u_1^D = \ddot{z}^d + \frac{K_z}{m} \dot{z}^d + a_3 \dot{e}_z + b_3 e_z$$

where \dot{u}_1^A , \dot{u}_1^B , \dot{u}_1^C , \dot{u}_1^D is:

$$\begin{aligned} \dot{u}_1^A &= \left[m (\cos \phi \cos \theta)^2 (\ddot{\phi} \sin \phi \cos \theta + \dot{\phi}^2 \cos \phi \cos \theta \right. \\ &\quad \left. - 2\dot{\phi}\dot{\theta} \sin \phi \sin \theta + \ddot{\theta} \cos \phi \sin \theta + \dot{\theta}^2 \cos \phi \cos \theta \right. \\ &\quad \left. + 2m \cos \phi \cos \theta (\dot{\phi} \sin \phi \cos \theta + \dot{\theta} \cos \phi \sin \theta)^2 \right] / (\cos \phi \cos \theta)^4 \end{aligned}$$

$$\dot{u}_1^B = \ddot{z}^d + \frac{K_z}{m} \dot{z}^d + a_3 \dot{e}_z + b_3 e_z \quad (30)$$

$$\dot{u}_1^C = u_1^A$$

$$\dot{u}_1^D = \ddot{z}^d + \frac{K_z}{m} \dot{z}^d + a_3 \dot{e}_z + b_3 e_z$$

By combining Equations (25) and (27), it can be solved that:

$$\begin{aligned} \ddot{\phi} &= (T_{1c}T_{2b} - T_{1b}T_{2c}) / (T_{1a}T_{2b} - T_{1b}T_{2a}) \\ \ddot{\theta} &= (T_{2c} - ((T_{1c}T_{2b} - T_{1b}T_{2c}) / (T_{1a}T_{2b} - T_{1b}T_{2a}))T_{2a}) / T_{2b} \end{aligned} \quad (31)$$

Equation (31) is combined with Equation (1) in the dynamic model, where $\ddot{\phi}$ and $\ddot{\theta}$, the control inputs u_2 and u_3 can be solved as follows:

$$\begin{aligned} u_2 &= \frac{I_x}{l} [(T_{1c}T_{2b} - T_{1b}T_{2c}) / (T_{1a}T_{2b} - T_{1b}T_{2a}) - \dot{\theta}\dot{\psi} \frac{I_y - I_z}{I_x} - \frac{J_r}{I_x} \dot{\Omega}_r + \frac{K_\phi l}{I_x} \dot{\phi}] \\ u_3 &= \frac{I_y}{l} [(T_{2c} - ((T_{1c}T_{2b} - T_{1b}T_{2c}) / (T_{1a}T_{2b} - T_{1b}T_{2a}))T_{2a}) / T_{2b} - \dot{\psi}\dot{\phi} \frac{I_z - I_x}{I_y} \\ &\quad + \frac{J_r}{I_y} \dot{\Omega}_r + \frac{K_\theta l}{I_y} \dot{\theta}] \end{aligned} \quad (32)$$

Regarding the dynamic and independent design of ψ , define $e_\psi = \psi^d - \psi$, that $\dot{e}_\psi = \dot{\psi}^d - \dot{\psi}$, $\ddot{e}_\psi = \ddot{\psi}^d - \ddot{\psi}$, setting:

$$\ddot{e}_\psi + a_4 \dot{e}_\psi + b_4 e_\psi = 0 \quad (33)$$

Equation (33) is combined with Equation (1) in the dynamic model, where $\ddot{\psi}$, the control inputs u_4 can be solved as follows:

$$u_4 = I_z (\ddot{\psi}^d + a_4 \dot{e}_\psi + b_4 e_\psi - \dot{\phi}\dot{\theta} \frac{I_x - I_y}{I_z} + \frac{K_\psi}{I_z} \dot{\psi}) \quad (34)$$

At this point, the dynamic inverse decoupling control design is completed, and four control inputs u_1 - u_4 are obtained.

3. Results and Discussion

This section discusses the simulation environment, parameter settings, and simulation experiment results and discussions.

3.1. Simulation Environment

This section uses Matlab software to simulate and verify the proposed dynamic inverse decoupling control strategy. By comparing it with the method proposed by Xiong et al. [34] and the classical PID control method in terms of energy consumption, the effectiveness and low energy consumption control characteristics of dynamic inverse decoupling control are demonstrated.

The Simulink block diagram constructed during the simulation process is shown in Figure 4.

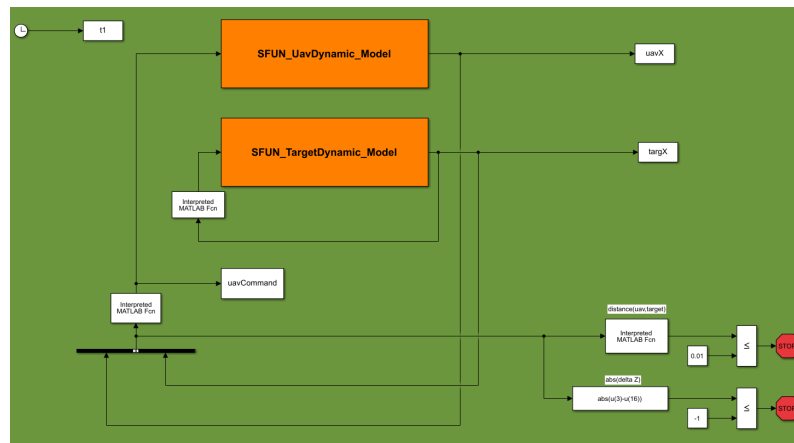


Figure 4. Simulink block diagram used for simulation.

3.2. Simulation Parameters

In the simulation environment, the model parameter settings of the quadcopter unmanned aerial vehicle in the dynamic inverse decoupling control proposed in this paper are shown in Table 2 (some parameters come from reference [34]), and the controller parameters are shown in Table 3.

Table 2. Parameter values for quadcopter unmanned aerial vehicle model.

Variable	Value	Units
m	2.0	kg
$I_x=I_y$	1.25	Ns^2/rad
I_z	2.2	Ns^2/rad
$K_x=K_y=K_z$	0.01	Ns/m
$K_\phi=K_\theta=K_\psi$	0.012	Ns/m
l	1.0	m
J_r	1.0	Ns^2/rad
b	2.0	Ns^2
d	5.0	Nms^2
g	9.8	m/s^2

Table 3. Controller parameter values.

Variable	Value
a_1	6.0
a_2	6.0
a_3	6.0
a_4	6.0
b_1	9.0
b_2	9.0
b_3	9.0
b_4	9.0
a_{11}	10.0
a_{22}	10.0
b_{11}	25.0
b_{22}	25.0

3.3. Simulation Results and Discussion

This section first conducted simulations on the effectiveness of dynamic inverse decoupling control, and then simulated the effectiveness of energy optimization in task scenarios.

3.3.1. Simulation of the Effectiveness of Dynamic Inverse Decoupling Control

Set the initial coordinate point of the drone to $(x_0, y_0, z_0) = (0, 0, 0)$, the initial attitude angle is $(\phi_0, \theta_0, \psi_0) = (0, 0, 0)$, the initial speed is $(v_{x0}, v_{y0}, v_{z0}) = (0, 0, 0)$. Since ψ^d is set separately, set $\psi^d = 0.5$. The target point adopts a particle motion model, and the coordinates of the target point are set as $(x, y, z) = (2, 2, 2)$. The angle between the velocity vector and the horizontal plane is set to 0° , and the angle between the horizontal plane projection and the ground x-axis is 30° .

The simulation results of the dynamic inverse decoupling control proposed in this article are as follows:

In the simulation environment of the above parameters and controller parameters, the flight trajectory of the quadcopter drone is shown in Figure 5, and the speed variation is shown in Figure 6. The simulation results show that the drone can accurately reach the set target point:

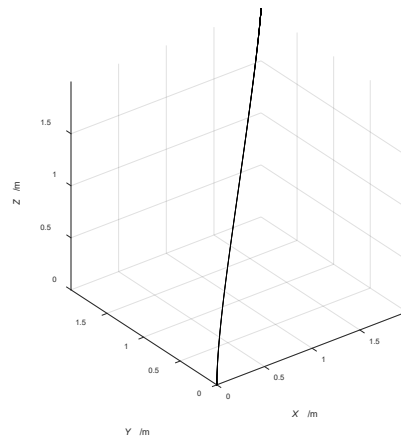


Figure 5. Quadcopter drone flight trajectory.

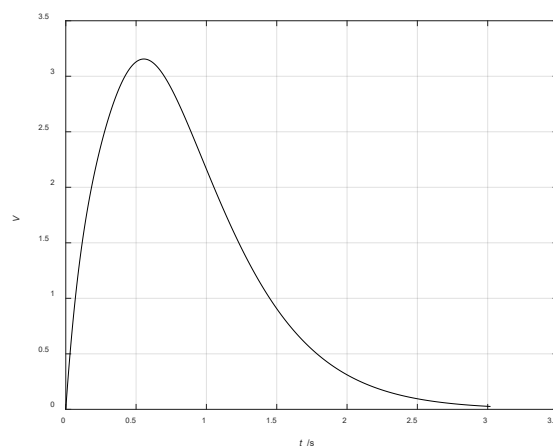


Figure 6. Speed variation of quadcopter unmanned aerial vehicle.

The changes in control inputs u_1-u_4 are shown in Figure 7:

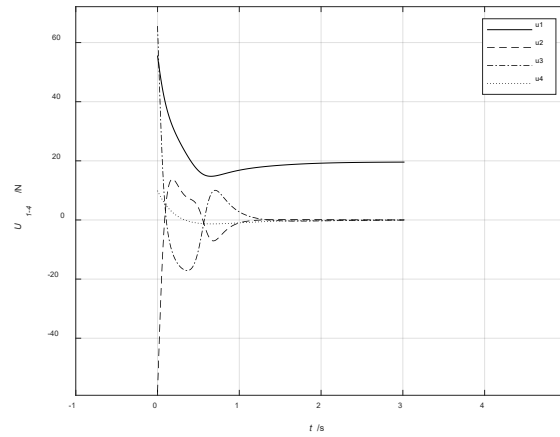


Figure 7. Control input u_1 - u_4 changes.

The speed variation of the quadcopter of the drone is shown in Figure 8:

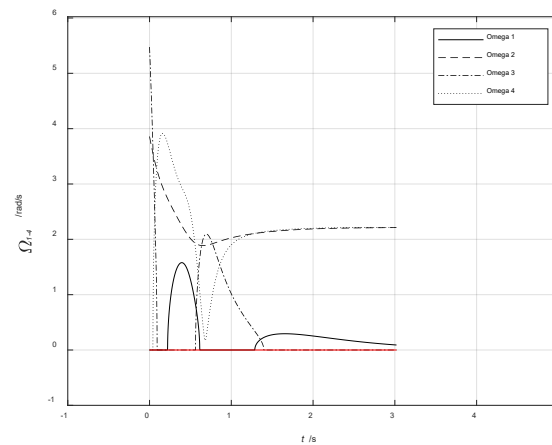


Figure 8. Rotation speed variation of quadcopter of unmanned aerial vehicle.

During the flight, the variation of the attitude angle ϕ, θ, ψ of the quadcopter unmanned aerial vehicle is shown in Figure 9-Figure 11. Simulation results show that the attitude angle of the unmanned aerial vehicle can eventually converge.

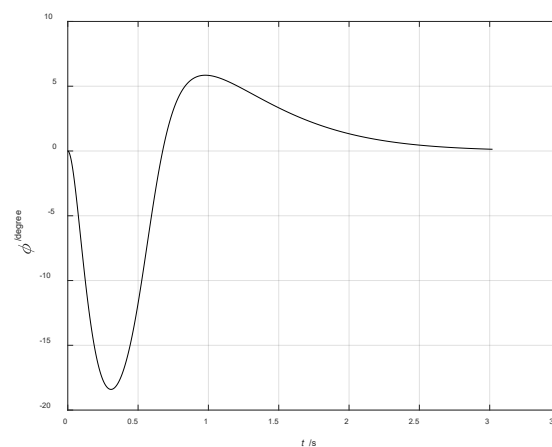


Figure 9. Drone ϕ angle change.

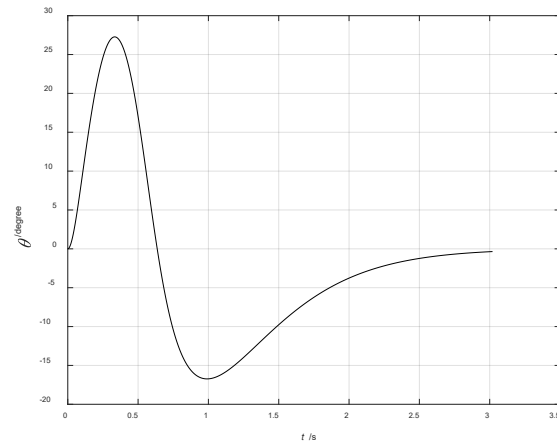


Figure 10. Drone θ angle change.

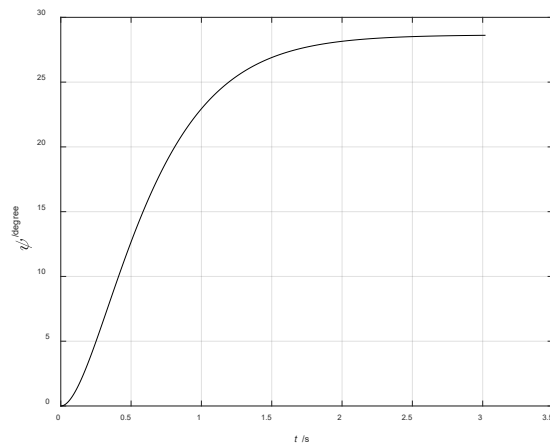


Figure 11. Drone ψ angle change.

The flight energy consumption of unmanned aerial vehicles under dynamic decoupling control is shown in Figure 12. The dashed line represents instantaneous energy consumption, and the solid line represents total flight energy consumption.

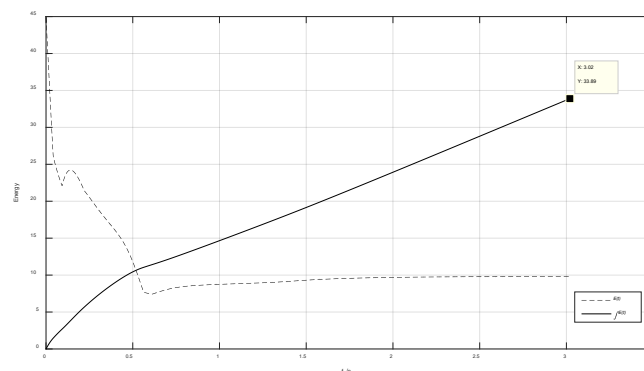


Figure 12. Energy consumption of unmanned aerial vehicle flight under dynamic inverse decoupling control.

Regarding the controller proposed in reference [34], the drone parameters are shown in Table 2. Under the same conditions, the drone flight energy consumption in the controller of reference [34] is

shown in Figure 13, where the dashed line represents instantaneous energy consumption and the solid line represents total flight energy consumption.

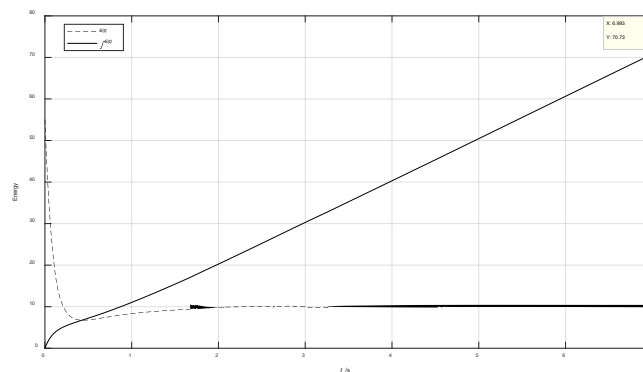


Figure 13. Reference [34] Energy consumption of unmanned aerial vehicle flight in controller.

For the classic PID control method, the parameters of the drone are shown in Table 2, and the PID parameters are shown in Table 4. Under the same conditions, the energy consumption of the drone during flight is shown in Figure 14, where the dashed line represents instantaneous energy consumption and the solid line represents total flight energy consumption.

Table 4. PID Parameter values.

Variable	Value
$K_{px}=K_{py}=K_{pz}$	0.05
$K_{dx}=K_{dy}=K_{dz}$	0.5
$K_{ix}=K_{iy}=K_{iz}$	0.0
$K_{p\phi}=K_{p\theta}$	1.0
$K_{d\phi}=K_{d\theta}$	2.0
$K_{i\phi}=K_{i\theta}$	0.1
$K_{p\psi}$	0.5
$K_{d\psi}$	1.0
$K_{i\psi}$	0.0

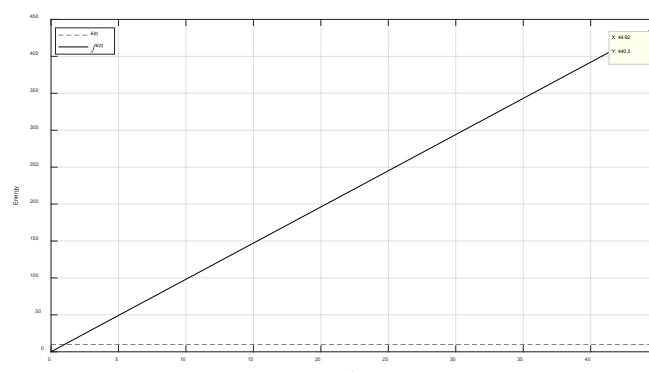


Figure 14. Energy consumption of unmanned aerial vehicle flight under classical PID control.

Based on Figure 12-Figure 14, the flight energy consumption of unmanned aerial vehicles can be obtained under dynamic inverse decoupling control, the controller in reference [34], and classical PID control. In order to better compare and reflect the energy consumption optimization control effect of

this article, the comparison chart of flight energy consumption under three states is shown in Figure 15.

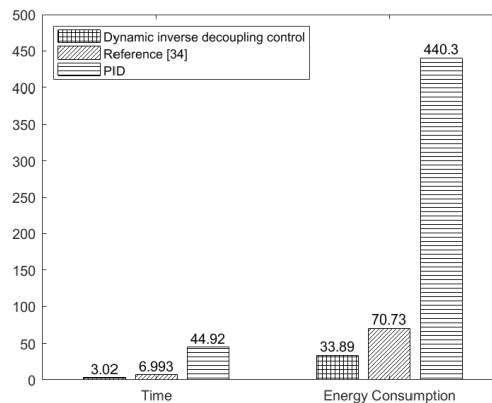


Figure 15. Comparison of flight energy consumption under three control states.

The simulation results show that the dynamic inverse decoupling control proposed in this paper can effectively save flight time and energy consumption under three control states, proving the effectiveness and low-energy control characteristics of the proposed decoupling control scheme.

3.3.2. Simulation of the Effectiveness of Energy Optimization in Task Scenarios

In order to verify the effectiveness of the proposed dynamic decoupling control in the task scenario of integrated air ground cooperation, simulation verification was conducted according to the set scenario and the above simulation steps and conditions.

Assuming there are three sensor nodes, the drone needs to start from the starting point and pass through three sensors in sequence for information collection or charging tasks. The sensor distribution is shown in Figure 16.

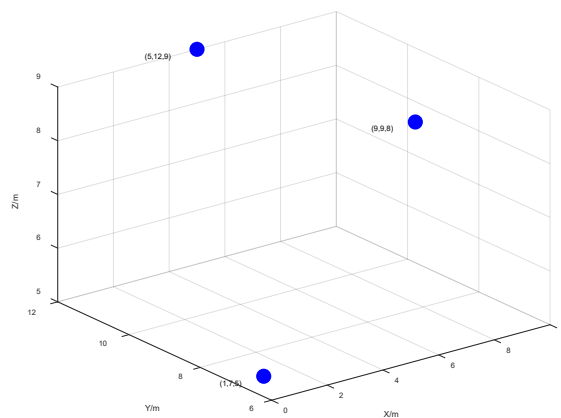


Figure 16. Sensor distribution.

According to the conditions and steps set in 3.3.1, the simulation was performed, and the obtained drone flight path is shown in Figure 17.

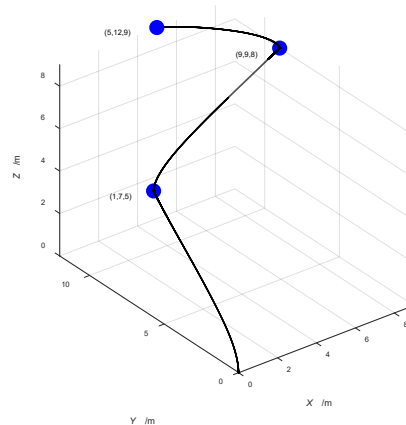


Figure 17. UAV flight path under dynamic inverse decoupling control task scenario.

The energy consumption of unmanned aerial vehicle flight under the same simulation and three control algorithms is shown in Table 5.

Table 5. Three control algorithms for drone flight energy consumption.

Control algorithm	Total flight energy consumption
Dynamic inverse decoupling control	150.9359 J
Reference [34]	311.7295 J
PID	1500.9461 J

It can be seen that in the scenario of integrated air ground collaborative tasks, the dynamic inverse decoupling control strategy proposed in this paper can still effectively reduce flight energy consumption and achieve energy optimization, verifying the effectiveness of the dynamic inverse decoupling control strategy under integrated air ground collaboration.

4. Conclusions

Based on the demand for energy consumption optimization of quadcopter unmanned aerial vehicles, this paper proposes a dynamic inverse decoupling control scheme to reduce its control energy consumption and achieve decoupling of motion channels. Firstly, by designing a direct closed-loop feedback control for the z-axis channel, it can exhibit an adjustable second-order linear dynamic response; Then, specific functions of pitch angle and yaw angle are combined as virtual control variables for decoupling design of the x-axis and y-axis channels, enabling both to have adjustable second-order linear dynamic characteristics. Afterwards, this article designed a calculation method for actual control variables to dynamically and quickly converge the deviation of virtual control variables to the desired value, ensuring control accuracy.

By comparing with other control methods (such as classical PID) in energy consumption simulation, the superiority and control performance of the proposed scheme in energy consumption have been verified, providing new ideas for low-energy control of quadcopter drones.

Author Contributions: Guoxin Ma: Conceptualization, methodology, formal analysis, project management, funding acquisition, paper framework; Kang Tian: Methodology derivation, simulation experiments, paper writing and editing; Hongbo Sun: Investigation, formal analysis, data organization, and funding acquisition; Yongyan Wang: Paper proofreading, software, supervision. All authors have read and agreed to the published version of the manuscript; Haitao Li: Paper verification and supervision.

Funding: This work is supported by the National Key R&D Program of China (Grant No. 2021YFE0111600).

Data Availability Statement: When using the data in this manuscript, readers can directly cite this manuscript or contact the authors for access.

Acknowledgments: This study would like to express special gratitude to the National Key Research and Development Program (2021YFE0111600) for its funding.

Conflicts of Interest: The authors declare no conflicts of interest.

References

1. Li, X.; Huang, G.; Wang, Z.; Zhao, B. Optics-driven drone. *Sci. China Inf. Sci.* **2024**, *67*, 124201.
2. Bartolomei, L.; Teixeira, L.; Chli, M. Fast Multi-UAV Decentralized Exploration of Forests. *IEEE Robot. Autom. Lett.* **2023**, *8*, 5576-5583.
3. Bassolillo, S.R.; D'Amato, E.; Notaro, I. A Consensus-Driven Distributed Moving Horizon Estimation Approach for Target Detection Within Unmanned Aerial Vehicle Formations in Rescue Operations. *Drones* **2025**, *9*, 127.
4. Jiang, C.X.; Yang, L.A.; Gao, Y.Q.; Zhao, J.; Hou, W.N.; Xu, F.M. An Intelligent 5G Unmanned Aerial Vehicle Path Optimization Algorithm for Offshore Wind Farm Inspection. *Drones* **2025**, *9*, 47.
5. Rad, S.S.; Zheng, Z.; Kheirollahi, R.; Mostafa, A.; Zhao, S.; Wang, Y.; Chevinly, J.; Nadi, E.; Bensala, T.; Zhang, H.; et al. Electromagnetic Interference on Unmanned Aerial Vehicles (UAVs): A Case Study of High Power Transmission Line Impacts. *IEEE Trans. Transp. Electrification* **2025**, 1-1.
6. Ahmed, M.; Soofi, A.A.; Raza, S.; Khan, F.; Ahmad, S.; Ullah, W.; Asif, M.; Xu, F.; Han, Z. Advancements in RIS-Assisted UAV for Empowering Multi-Access Edge Computing: A Survey. *IEEE Internet Things J.* **2025**, 1-1.
7. Cao, P.; Lei, L.; Cai, S.; Shen, G.; Liu, X.; Wang, X.; Zhang, L.; Zhou, L.; Guizani, M. Computational Intelligence Algorithms for UAV Swarm Networking and Collaboration: A Comprehensive Survey and Future Directions. *IEEE Commun. Surv. Tutor.* **2024**, *26*, 2684-2728.
8. Xu, S.; Zou, N.; He, Q.; He, X.; Li, K.; Cheng, M.; Liu, K. Design and Application Research of a UAV-Based Road Illuminance Measurement System. *Automation* **2024**, *5*, 407-431.
9. Lang, M.; Antsov, M.; Mumma, A.; Suitso, I.; Kuusk, A.; Piip, K. Comparison of forest canopy gap fraction measurements from drone-based video frames, below-canopy hemispherical photography, and airborne laser scanning. *Eur. J. Remote Sens.* **2025**, *58*, 2456629.
10. Qu, H.; Zheng, C.; Ji, H.; Barai, K.; Zhang, Y.-J. A fast and efficient approach to estimate wild blueberry yield using machine learning with drone photography: Flight altitude, sampling method and model effects. *Comput. Electron. Agric.* **2024**, *216*, 108543.
11. Ri, S.; Ye, J.; Xia, P.; Toyama, N.; Ogura, N.; Shiotani, T. Bridge deflection measurement by drone aerial photography using the sampling moiré method. In Proceedings of the International Conference on Optical and Photonic Engineering (icOPEN 2023), Singapore, Singapore, 15 February 2024; pp. 168-171.
12. Gao, J.; Wang, Q.; Li, Z.; Zhang, X.; Hu, Y.; Han, Q.; Pan, Y. Toward Efficient Urban Emergency Response Using UAVs Riding Crowdsourced Buses. *IEEE Internet Things J.* **2024**, *11*, 22439-22455.
13. De Lucia, L.; Palazzi, C.E.; Vegni, A.M. ENSING: Energy saving based data transmission in Internet of Drones for 3D connectivity in 6G networks. *Ad Hoc Netw.* **2023**, *149*, 103211.
14. Cariou, C.; Moiroux-Arvis, L.; Bendali, F.; Mailfert, J. Optimal route planning of an Unmanned Aerial Vehicle for data collection of agricultural sensors. In Proceedings of the IEEE INFOCOM 2024-IEEE Conference on Computer Communications Workshops (INFOCOM WKSHPS), Vancouver, BC, Canada, 20-20 May 2024; pp. 1-6.

15. Wu, Y.; Yin, H.; Chen, X.; Zhang, M. Multicircuit Route Planning for UAVs Performing the Terrain Coverage Task. *IEEE Internet Things J.* **2024**, *11*, 23765-23779.
16. Alyassi, R.; Khonji, M.; Karapetyan, A.; Chau, S.C.K.; Elbassioni, K.; Tseng, C.M. Autonomous Recharging and Flight Mission Planning for Battery-Operated Autonomous Drones. *IEEE Trans. Autom. Sci. Eng.* **2023**, *20*, 1034-1046.
17. Wan, P.; Wang, S.; Xu, G.; Long, Y.; Hu, R. Hybrid Heuristic-Based Multi-UAV Route Planning for Time-Dependent Data Collection. *IEEE Internet Things J.* **2024**, *11*, 24134-24147.
18. Wang, X.; Ma, T.; Zhang, L.; Qiao, N.; Xue, P.; Fu, J. Multi-Phase Trajectory Planning for Wind Energy Harvesting in Air-Launched UAV Swarm Rendezvous and Formation Flight. *Drones* **2024**, *8*, 709.
19. Hadid, S.; Boushaki, R.; Boumchedda, F.; Merad, S. Enhancing Quadcopter Autonomy: Implementing Advanced Control Strategies and Intelligent Trajectory Planning. *Automation* **2024**, *5*, 151-175.
20. Ferrusquia, A.; Guo, W. Reservoir Computing for Drone Trajectory Intent Prediction: A Physics Informed Approach. *IEEE T. Cybern.* **2024**, *54*, 4939-4948.
21. Zhuang, X.; Li, D.; Wang, Y.; Liu, X.; Li, H. Optimization of high-speed fixed-wing UAV penetration strategy based on deep reinforcement learning. *Aerosp. Sci. Technol.* **2024**, *148*, 109089.
22. Carvajal, C.P.; Andaluz, V.H.; Varela-Aldás, J.; Roberti, F.; Del-Valle-Soto, C.; Carelli, R. Visual Servoing Using Sliding-Mode Control with Dynamic Compensation for UAVs' Tracking of Moving Targets. *Drones* **2024**, *8*, 730.
23. Kumar, S.; Yesmin, A.; Sinha, A.; Guha, A. Adaptive Continuous Terminal Sliding Mode Control for Unmanned Aerial Vehicle. In Proceedings of the 2024 Tenth Indian Control Conference (ICC), Bhopal, India, 09-11 December 2024; pp. 262-267.
24. Admas, Y.A.; Mitiku, H.M.; Salau, A.O.; Omeje, C.O.; Braide, S.L. Control of a fixed wing unmanned aerial vehicle using a higher-order sliding mode controller and non-linear PID controller. *Sci Rep* **2024**, *14*, 23139.
25. Yu, H.; Miao, K.; He, Z.; Zhang, H.; Niu, Y. Fault-Tolerant Time-Varying Formation Trajectory Tracking Control for Multi-Agent Systems with Time Delays and Semi-Markov Switching Topologies. *Drones* **2024**, *8*.
26. Lee, B.; Hyun, D.; Kim, J.; Lee, S.; Ban, J. Design of Robust H^∞ Guaranteed Cost Controller of Quadrotor UAV for Set-Point Tracking. *IEEE Access* **2024**, *12*, 126074-126087.
27. Xing, S.; Zhang, X.; Tian, J.; Xie, C.; Chen, Z.; Sun, J. Morphing Quadrotors: Enhancing Versatility and Adaptability in Drone Applications—A Review. *Drones* **2024**, *8*.
28. Wu, Y.; Chen, M.; Li, H.; Chadli, M. Event-Triggered-Based Adaptive NN Cooperative Control of Six-Rotor UAVs With Finite-Time Prescribed Performance. *IEEE Trans. Autom. Sci. Eng.* **2024**, *21*, 1867-1877.
29. Liu, S.; Jiang, B.; Mao, Z.; Zhang, Y. Distributed adaptive event-triggered fault-tolerant cooperative control of multiple UAVs and UGVs under DoS attacks. *IET Contr. Theory Appl.* **2023**, *18*, 2296-2306.
30. Amerttet, S.; Gebresenbet, G.; Alwan, H.M. Modeling of Unmanned Aerial Vehicles for Smart Agriculture Systems Using Hybrid Fuzzy PID Controllers. *Appl. Sci.-Basel* **2024**, *14*, 3458.
31. Tassanbi, A.; Ali Khan, A.; Kashkynbayev, A.; Shehab, E.; Duc Do, T.; Ali, M.H. Performance evaluation of developed controllers for unmanned aerial vehicles with reference camera. *Meas. Control* **2024**, 00202940241270863.
32. Zhao, H.; Fu, H.; Yang, F.; Qu, C.; Zhou, Y. Data-driven offline reinforcement learning approach for quadrotor's motion and path planning. *Chin. J. Aeronaut.* **2024**, *37*, 386-397.
33. Yao, J.; Rafee Nekoo, S.; Xin, M. Approximate optimal control design for quadrotors: A computationally fast solution. *Optim. Control Appl. Methods* **2023**, *45*, 85-105.

34. Xiong, J.J.; Zheng, E.H. Position and attitude tracking control for a quadrotor UAV. *ISA Trans.* **2014**, *53*, 725-731.
35. Li, B.; Li, Q.; Zeng, Y.; Rong, Y.; Zhang, R. 3D Trajectory Optimization for Energy-Efficient UAV Communication: A Control Design Perspective. *IEEE Trans. Wirel. Commun.* **2022**, *21*, 4579-4593.

Disclaimer/Publisher's Note: The statements, opinions and data contained in all publications are solely those of the individual author(s) and contributor(s) and not of MDPI and/or the editor(s). MDPI and/or the editor(s) disclaim responsibility for any injury to people or property resulting from any ideas, methods, instructions or products referred to in the content.